

Highly Stable Strontium Fluoride as a Thickness Tolerant Electron-Selective Contact for Dopant-Free Silicon Solar Cells

Wenxian Wang¹, Lun Cai², Lanxiang Meng², Nuo Chen², Huiqi Wei², Yang Hong², Yongjuan Chen², Linyi Zeng², and Zongcun Liang¹

¹Sun Yat-Sen University

²Affiliation not available

November 8, 2023

Abstract

Commercialized passivated emitter and rear cell (PERC) silicon solar cells feature direct contact of metal with silicon, which leads to severe recombination loss and low open circuit voltage (V_{oc}). To overcome the loss, the authors demonstrate a highly stable and thickness-tolerant dopant-free electron-selective contact consisting of a strontium fluoride/aluminium (SrF_2/Al) stack. The inserting dielectric SrF_2 layer can mitigate the Fermi-level pinning effect between the silicon substrate and the Al electrode. Besides, a comparatively small Ohmic contact resistivity of $2 \text{ m}\Omega\text{-cm}^2$ on lightly doped n-type c-Si can be achieved when using 4 nm of SrF_2 . Moreover, the formed contact within 9 nm SrF_2 is stable for over 5000 hours in the air without encapsulation. Solar cells with this novel dopant-free electron-selective contact reach a power conversion efficiency (PCE) of 21.56%. The promising results and its stable nature, indicate its potential to serve as cost-efficient electron-selective contact for various optoelectronic devices.

1. Introduction

The development of the solar cell preparation process gradually shifted from a complex process and high energy consumption to a route of the reduced preparation process and low energy consumption. At the same time, silicon solar cells have undergone evolution resulting in traditional Al-back surface field cells (Al-BSF cells),¹ PERC cells,^{2,3} tunnel oxide passivating contact (TOPCon),^{4,5} heterojunction with intrinsic thin-layer (HIT).⁶ Among them, the HIT solar cell is one of the most typical examples of low-temperature fabrication routes. However, it still has four problems that need to be solved: a) The a-Si:H emitters must be heavily doped utilizing flammable and toxic gas precursors such as boranes and phosphine. b) The rather narrow direct band gap of approximately 1.7 eV in a-Si:H layers results in significant parasitic absorption of UV and blue light., which requires precise thickness control. c) The required plasma-enhanced chemical vapor deposition (PECVD) results in high manufacturing costs, which impedes the spread of solar cell technology. d) Needs of low-temperature metallization process.

Dopant-free carrier-selective contacts have gained great attention to the c-Si solar cells research community recently because they can significantly reduce optical parasitic absorption and simplify the fabrication process as compared to silicon heterojunction cell architecture.⁷ Most of those materials are large-band-gap chemical compounds and can be divided into dopant-free hole carrier-selective contacts (DF-HCSCs) and electron carrier-selective contacts (DF-ECSCs) depending on their functions. DF-HCSCs materials usually have ultra-high work functions forming up-bending valence band which promotes hole transport. The typical examples are transition metal oxides or nitrides such as MoO_x , WO_3 , V_2O_x , CrO_x , and TiN_x .⁸⁻¹¹ PEDOT:PSS as organic DF-HCSCs also have been extensively explored on silicon solar cells.¹² The highest PCE of dopant-free silicon heterojunction (SHJ) solar cells is 23.83% achieved by plasma treatments 1.7 nm thick of MoO_x layer as the hole-selective contact.¹³

DF-ECSC materials have been investigated as interface modification layers in SHJ solar cells due to their very low work function. Typical examples of DF-ECSCs are alkaline-earth metal salts such as LiF_x , CsF , Cs_2CO_3 , TiO_x , MgF_x and rare-earth compounds like EuF_3 , GdF_3 , and CeF_3 .^{7,14-23} Moreover, polymers like branched polyethyleneimine, Triton X-100, and MgAcac are reported as DF-ECSCs.²⁴⁻²⁶ Among them, the LiF_x is one of the most typical DF-ECSCs materials. This interest sparked in 2016 when an SHJ solar cell with a front a-Si:H(i)/ MoO_3 /ITO and rear a-Si:H(i)/ LiF_x /Al structure achieved an efficiency of 19.42%.⁷

Nevertheless, The development of the DF-ECSCs technology has been hindered by the severe degradation of LiF_x /Al ECSCs. Additionally, the efficiency (23.07%) of the solar cells and their stability tolerance were improved by incorporating a shielded TiO_2 (1.5 nm) layer between the a-Si:H passivating layer and the low work function (WF Φ) LiF_x /Al electrodes().²⁷ However, the poor thickness-tolerant of LiF_x becomes another challenge for function as a DF-ECSC in the long-term run. The thickness of the LiF_x stack must be carefully controlled at 1~2 nm to ensure effective tunneling. In addition, lithium compounds materials are expensive and toxic, which harms human health. Besides, the lack of long-term stability studies is also a shortcoming for most reported electron-selective contacts.

An approach that has great potential to mitigate these mentioned disadvantages is to apply healthcare DF-ECSC materials. Strontium fluoride (SrF_2) has been widely used in toothpaste being an annexing agent in our daily life.²⁸ It is also reported in light-emitting devices, optical imaging, and anion conductors thanks to its low energy phonon, high ionization, and good anion conductivity.²⁹ Recently, it has been revealed that SrF_2 can act as a buffer layer in organic solar cells to increase efficiency as a cathode interlayer.³⁰ But the utilization of SrF_2 for c-Si solar cells has not been researched in the current state of research. In this contribution, we developed thickness-tolerant and highly stable DF-ECSCs for c-Si by introducing 1.5 ~ 9 nm thermal evaporated SrF_2 films. The use of X-ray photoelectron spectroscopy (XPS) indicates that the SrF_2 film, fabricated through thermal evaporation, is stoichiometric. Ultraviolet photoelectron spectroscopy (UPS) measurements indicate that the thin film exhibits an ultralow work function. The morphology and element distribution of the interface were investigated using high-resolution transmission electron microscopy (HRTEM) and energy-dispersive X-ray spectroscopy (EDX). The optimized solar cells with 4 nm SrF_2 located partially on the rear side exhibit a champion efficiency of 21.56%. Lastly, the SrF_2 /Al contact is shown to be stable beyond 5000 hours in the ambient air, demonstrating that SrF_2 is a prominent DF-ECSCs layer for cost-efficiency solar cells.

2. Results and Discussion

2.1. Photoelectron Spectroscopy of the SrF_2 Thin Film.

The chemical state and compositions of the deposited SrF_2 thin films on polished c-Si(n) were characterized by XPS. The surface contamination C 1s (284.8 eV) was used as a calibration standard for the binding energies of the whole input. The core level spectrums of F and Sr are illustrated in Figure 1. Figure 1A depicts the principal peak of the F 1s spectra at 684.7 eV. Two peaks are observed in the core level of the Sr 3d spectrum, as shown in Figure 1B. The Sr 3d_{5/2} main peak is at 133.6 eV binding energy. The peak at a binding energy of 135.5 eV is ascribed to the Sr 3d_{3/2}. Both characterization results were well consistent with the previous reports of SrF_2 thin films.³¹ The atomic ratio of F divided by Sr is obtained from the core-level peak areas. The relative sensitivity factor of a fraction is 1.92, demonstrating it is approximately stoichiometry.

As shown in Figure 1C,D, the SrF_2 work function and valence band were characterized by ultraviolet photoelectron spectroscopy (UPS) using a He I discharge source (21.22 eV). An Au reference sample has been used to calibrate the equipment before testing. Figure 1C indicates the WF (P') of the fabricated SrF_2 films is 2.80 eV through the secondary electron cut-off vicinity, which is lower than the reported electron selective materials LiF_x , TiO_2 , CeF_3 , and reference Al (4.1 eV) in the literature.^{7,18,22,32} Figure 1D shows the huge valence band offset of 7.1 eV between the Fermi energy level and the valence band maximum of the SrF_2 film, which can effectively block the holes' transport. The wide band gap of SrF_2 is around 7.55 eV

as generally reported in kinds of literature.^{33,34} It can be valued that the gap between the Fermi level and the electron affinity is 0.4 eV, leading to a small conduction band offset to lightly doped c-Si(n), benefiting the electron extraction from the conduction band by thermionic emission and tunneling. Thus, by inserting the SrF₂ layer, the Fermi-level pinning effect at the c-Si(n)/Al interface could be eliminated, increasing the driving power for the photo-generated carriers' separation, and confirming the outstanding ECSCs nature of n-type c-Si.

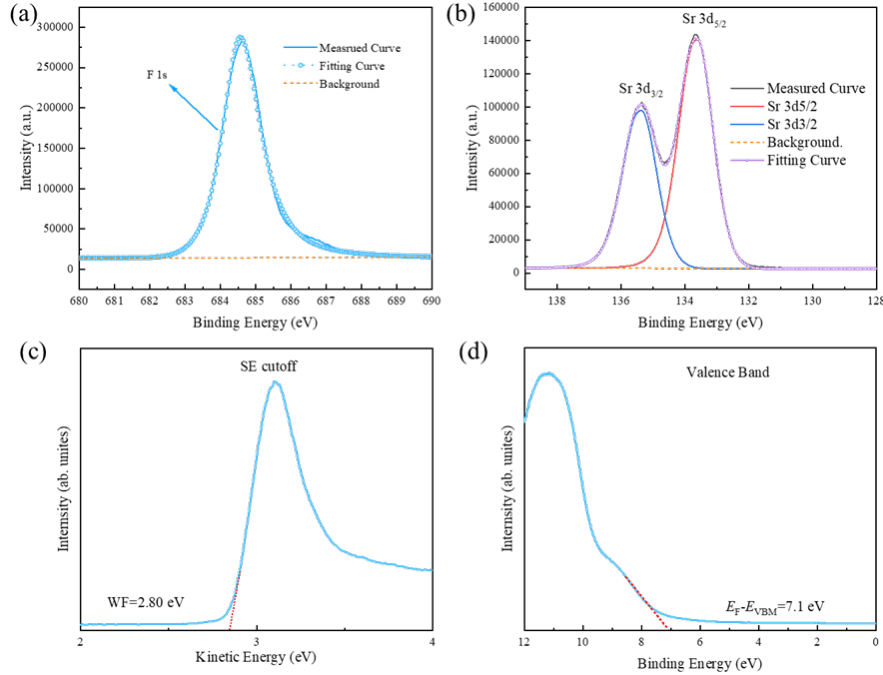


Figure 1: This is a caption

FIGURE 1 The thermally evaporated SrF₂ film was characterized using XPS and UPS measurements, as shown in the following statistics: (A) F 1s core level spectrum. (B) Sr 3d core spectrum. (C) Extracted WF of SrF₂ from the secondary electron cut-off spectrum. (D) Valence band spectrum of the SrF₂ film.

2.2. Contact Resistivity and Stability.

The contact resistivity (ρ_c) of the c-Si(n)/SrF₂/Al stack is a key factor in evaluating its electron selectivity ability. It was evaluated by the transfer length method (TLM) in Figure 2, with a schematic of the test structure inset.³⁵ The Schottky barrier height (> 0.7 eV) is caused by the potent Fermi-level pinning effects when an aluminum electrode is in straight contact with the lightly doped n-Si and behaves in a rectifying fashion. By contrast, Figure 2A exhibits that the interposition of a nanoscale SrF₂ thin film between the c-Si(n) substrate and aluminum electrode considerably enhances the contact presence and permits an Ohmic contact. The value of ρ_c is calculated as 2 m Ω [?]cm² from the 4 nm SrF₂/Al stack, which is lower than the great majority of other dopant-free structures in c-Si solar cells. DF-ECSCs works in kinds of literature report that the minimum ρ_c can be achieved by EuF_x (15.6 m Ω ·cm²), YF₃ (17.8 m Ω ·cm²), MgO_x (17.5 m Ω ·cm²), CeF₃ (10.96 m Ω ·cm²), MgAcac (7.6 m Ω ·cm²), MgF_x (35 m Ω ·cm²), TiO₂ (20 m Ω ·cm²), TaN_x (42 m Ω ·cm²) prepared by thermal evaporation or by atomic layer deposition (ALD).^{11,18-20,22,26,36,37} And the value of ρ_c resembles the most typical material LiF_x (1 m Ω ·cm²).⁷ However, lithium fluoride is toxic and harmful to human health and the environment, and Li resources and its compounds are in short supply on Earth, which is not conducive to large-scale applications. In contrast, SrF₂ is commonly used as an additive for toothpaste in humans' daily lives, which is non-toxic to physical health and the environment. Hence, it

has more prospects for large-scale application. The low ρ_c formed by n-Si/SrF₂/Al may be attributed to the lower WF of SrF₂. The energy band of c-Si(n) is forced to bend downwards further as Fermi depinning, which makes it easier for an electron aggregation area to form, thereby realizing the selective transmission of electrons.^{22,38}

It can be seen in Figure 2B that ρ_c remains in Ohmic contact ($< 42 \text{ m}\Omega\cdot\text{cm}^2$) as the thickness of SrF₂ varies from 1.5, 4, 6, to 9 nm, indicating its high tolerance for thickness, thus providing a wide processing window. By contrast, the most researched electron-selective structures, n-Si/LiF_x/Al and n-Si/MgO_x/Al have a narrow manufacturing window ($1.5 \pm 0.5 \text{ nm}$). The contact resistance stability of these c-Si/SrF₂/Al stack samples under air storage was investigated. Despite being exposed for 168 hours, the ρ_c is still less than $45 \text{ m}\Omega\cdot\text{cm}^2$ for all thicknesses investigated. Moreover, the ρ_c for SrF₂ within 9 nm remains below $140 \text{ m}\Omega\cdot\text{cm}^2$ over one and a half years. The results indicate that SrF₂ has considerable potential as a material for DF-ECSCs in c-Si solar cells, making it a promising candidate for large-scale manufacturing.

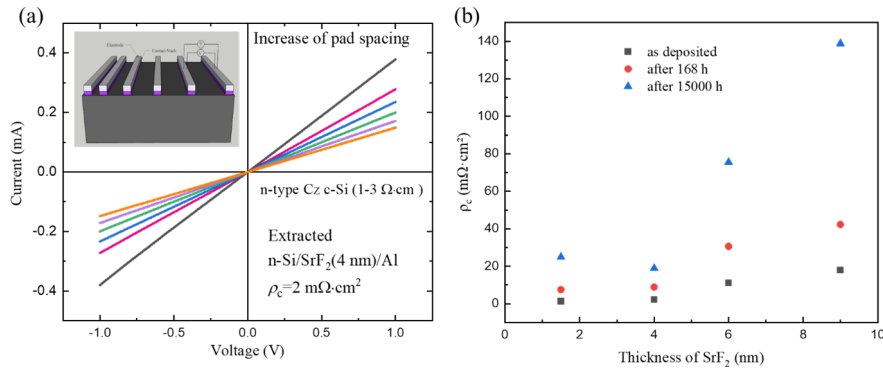


Figure 2: This is a caption

FIGURE 2 Contact resistivity values of SrF₂/Al stack associated with n-Si measured by the TLM. (A) The dark current-voltage measurement was performed on a structure consisting of a 1.5 nm SrF₂ film deposited on 1-3 Ω·cm lightly doped n-type c-Si and an Al layer. (B) The contact resistance of the structure was measured for various thicknesses of SrF₂ film, and the effect of storage time in the air was also examined.

2.3. n-Si/SrF₂/Al Interface.

To further investigate the cause of its high stability and thickness tolerance property. The scanning transmission electron microscopy-high-angle annular dark field (STEM-HAADF) technique was used in combination with energy-dispersive X-ray spectroscopy (EDXS) and electron-energy loss spectroscopy (EELS) to examine the interfacial structures and chemical elements at the n-Si/SrF₂/Al interface. As shown in Figure 3A, the microscopy images of the stack contact interface apparently visualize a homogeneous continuous SrF₂ interlayer, and n-Si is obviously recognizable. The thickness of the SrF₂ film is 4 nm calculated by the resolution scale, which is in accord with the deposition. The 1 nm SiO_x layer is usually produced by natural oxidation during a prolonged evacuation after the sample is transferred to the thermal evaporation chamber, which probably passivated the dangling bond of the Si surface³⁹. The EDXS maps of the n-Si/SrF₂/Al contact are presented in Figure 3b with a 20 nm resolution. The presence of the SrF₂ and SiO_x layers was verified by the elemental signals for Al, Sr, F, O, and Si. The top Al and bottom Si are separated by the Sr and F elements. In Figure 3C, the EELS signals of Sr and F fluctuate in the SrF₂ interlayer indicating that the interlayer is a combination of SrF₂ and a significant amount of Al (16 – 46%, absolute atomic percentage). This phenomenon is probably caused by the diffusion of SrF₂ film to the Al layer. Al atom mixtures have the potential to improve interlayer conductivity and provide a modest thickness dependency. The fabrication of c-Si/GdF₃/Al and vertical transistors using 2D materials has also shown similar behavior.^{40,41}

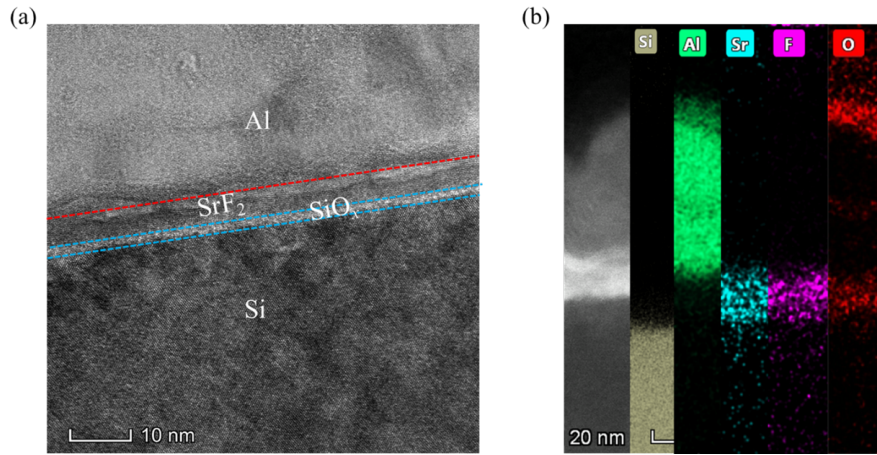


Figure 3: This is a caption

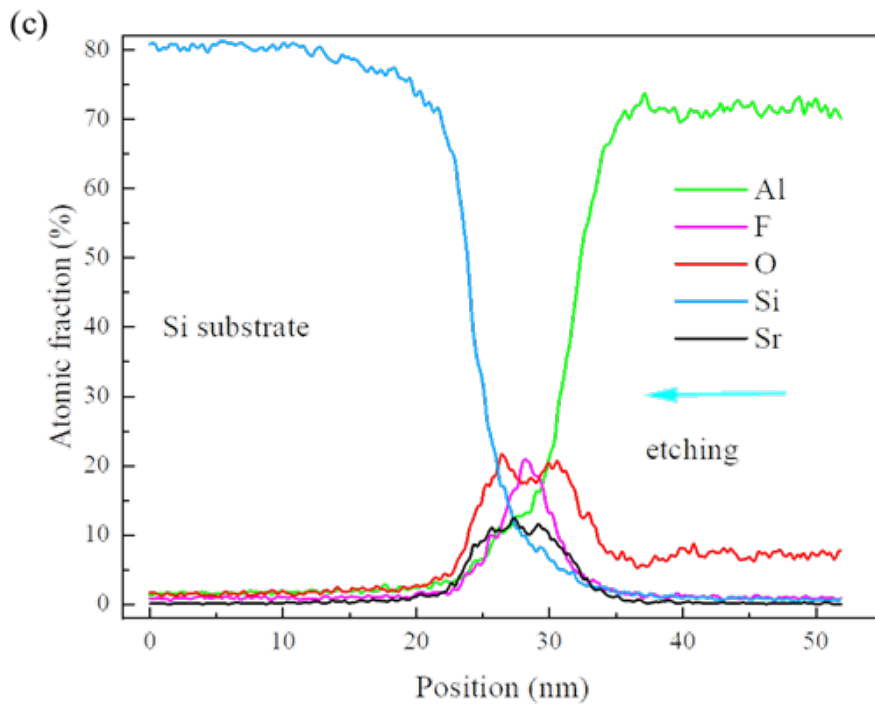


Figure 4: This is a caption

FIGURE 3 The interface images between c-Si(n)/SiO_x/SrF₂/Al were observed using STEM-HAADF (A) A high-resolution STEM HAADF microscopy picture of the n-Si/SrF₂/Al/ stack. (B) EDX mapping was performed with a 10 nm resolution for the signals of Al, Sr, F, and Si. (C) An EDX line scan was performed across the interfaces.

2.4. Proof-of-Concept n-Type Si Solar Cells.

To demonstrate the effect of the SrF₂/Al electron-selective on silicon solar cells' performance, The authors successfully produced a series of proof-of-concept c-Si solar cells on the n-type substrates with the partial

area rear SrF_2/Al contact architecture. Figure 4A illustrates a schematic diagram of an n-Si solar cell. To accomplish passivation and improve optical performance, the emitter of the fabricated solar cells was coated with an $\text{Al}_2\text{O}_3/\text{SiN}_x$ stack fabricated by PECVD. In Figure 4B, V_{oc} increases from 622 mV with Al contact directly to 645 after inserting a 2 nm SrF_2 layer. Then, the V_{oc} reaches its peak at 654 mV for the 4 nm SrF_2 layer and remains at a slight drop but still above 650 mV. The observed improvement in the performance of the solar cell can be explained by the decrease in recombination, which is due to the Fermi-level depinning effect occurring at the Al/n-Si interface.³⁸ The V_{oc} of the solar cell with illumination intensity has also been characterized to further demonstrate the removing Schottky barrier phenomenon (Figure S1). The fill factor (FF) and short-circuit current (J_{sc}) values depict a similar trend, as shown in figures 4C and D. The values fall as increasing the SrF_2 thickness beyond 4 nm, which is identified with the trend with contact resistance. Figure 4E depicts the PCE of the fabricated devices with various SrF_2 layer thicknesses.

Figure 4F compares the J - V characteristics obtained under 1 sun illumination of both cells with and without the optimal inserting layer SrF_2 (4 nm). The PCE of the fabricated solar cell was increased from 18.06% to 21.56%, indicating that it has the potential to be a new potential representative DF-ECSC for dopant-free silicon solar cells. This device has a V_{oc} of 654 mV, J_{sc} of 41.91 $\text{mA}\cdot\text{cm}^{-2}$, and FF of 78.68%. Due to the low contact resistance, the FF increased by 7.88% in comparison to the reference cell with Al contact directly. Both V_{oc} and J_{sc} saw a small performance improvement (from 622 mV, 40.98 $\text{mA}\cdot\text{cm}^{-2}$ to 654 mV, 41.91 $\text{mA}\cdot\text{cm}^{-2}$).

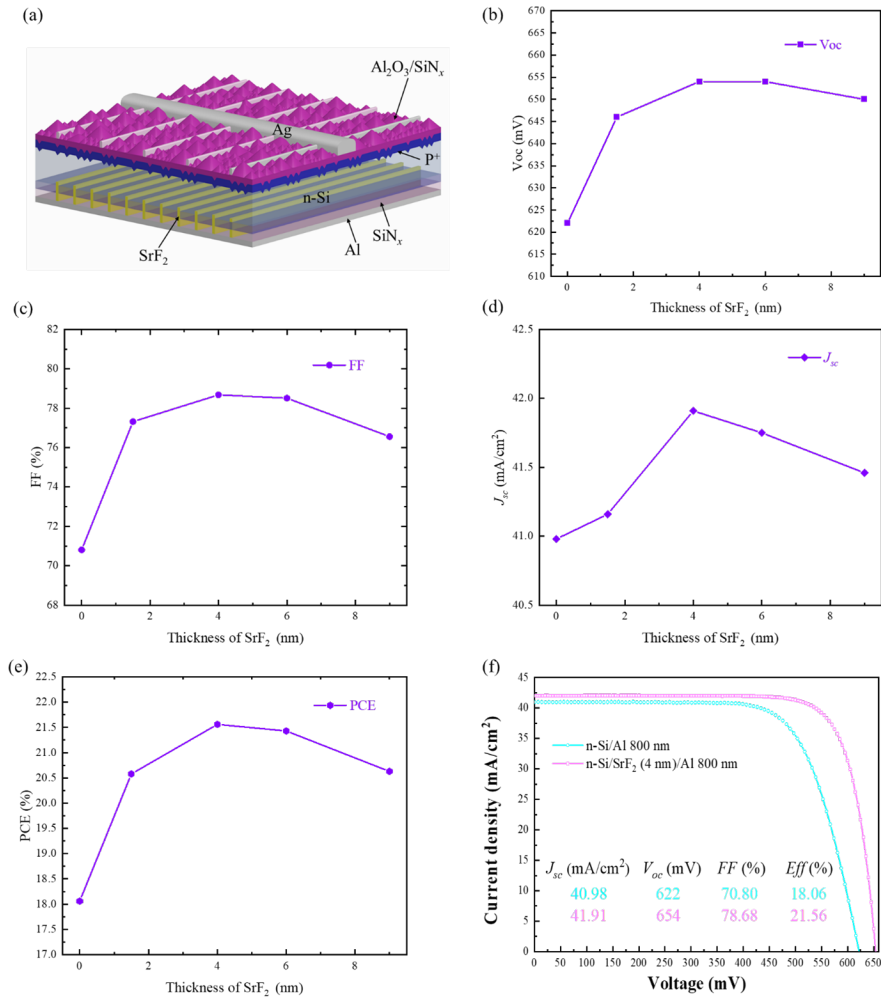


Figure 5: This is a caption

FIGURE 4 Device performance with partial rear SrF₂ films. (A) A sketch of the solar cells applying SrF₂ electron-selective contacts. (B-E) V_{oc} , FF, J_{sc} , and PCE of the device with various SrF₂ thicknesses (nm). (F) Light J - V characteristics of the device under AM1.5 conditions.

To evaluate the optical properties of SrF₂ electron selective contacts when applied on PERC structure solar cells. Figure 5A depicts the characterized EQE, reflectance of the highest efficiency device, and its relevance, with the measurements were taken between the finger electrode.

Obviously, a considerably high integration J_{sc} of the EQE of 42.30 mA[?] cm^{-2} was achieved, surpassing the J_{sc} value of the counterpart solar cell which was 41.32 mA[?] cm^{-2} . These findings are consistent with the J_{sc} values obtained from the J - V characterization discussed earlier. The optical quality of the back side can be indicated by the internal quantum efficiency (IQE) for longer wavelengths (900 ~ 1200 nm). A higher IQE is observed at wavelengths between 500 nm and 1200 nm for cells with SrF₂ interlayer than in the case of the cells only metalized by Al backside. This maybe indicates that SrF₂ film increases the spectral response and light reflection at its interfaces to the Si bulk, demonstrating the high electron selectivity characteristics offered by the low WF SrF₂/Al contacts.

The stability of PCE is an essential factor to consider when evaluating the practical application of a solar

cell. The champion samples were surveyed and stored in an ambient atmosphere as shown in Figure 5B. The PCE can remain constant for the first 168 hours at 21.5%. Then, a tiny decline can be seen, but it is still close to 21% after 1000 hours. The PCE was maintained at 17% to 17.5% even after samples were exposed to the air for 5000 hours and 15000 hours. We identify several potential causes for this phenomenon: (i) the increasing contact resistivity in Figure 2b. and (ii) the advent of Al diffusion into the silicon substrate of the electron-selective contact layer can lead to a rectifying contact, as has been widely reported in the literature.^{36,42} The stability of this structure could be further enhanced after module encapsulation. The use of SrF₂ as DF-ECSCs presents significant potential for mass manufacture due to its excellent PCE stability and high tolerance to variations in thickness during fabrication.

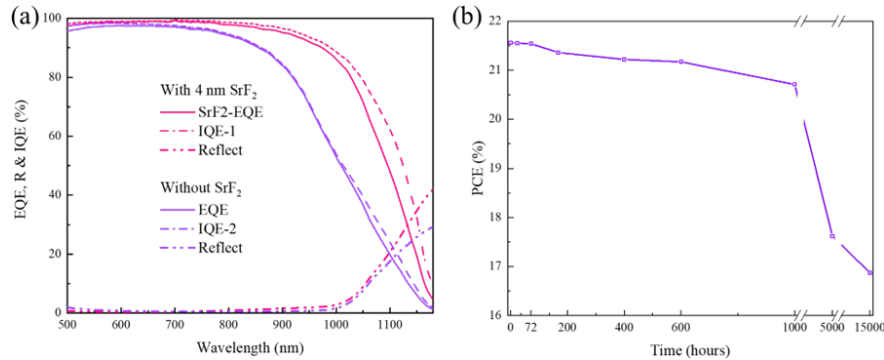


Figure 6: This is a caption

FIGURE.5 (A) The EQE, reflectance, and IQE measurements of the solar cells. (B) The stability of the champion PCE device in an ambient atmosphere.

3. Conclusion

The potential of SrF₂ thin films as a dopant-free and non-toxic electron-selective contact for silicon solar cells has been explored. The n-Si/Al interface's Fermi-level pinning effect was alleviated by inserting a thermally evaporated SrF₂ layer. The ultra-low work function quality enhances the electron selectivity and enables the contact resistivity to achieve 2 mΩ·cm² for an adjusted 4 nm SrF₂. In comparison to other known electron-selective contact materials, the SrF₂/Al contact exhibits exceptional stability and thickness tolerance. A dopant-free electron-selective contact consisting of SrF₂/Al layer was implemented in an n-type PERC solar cell, which achieved a champion efficiency of 21.56%. Our research findings confirm the outstanding electron-selective contact nature of SrF₂ for fabricating dopant-free silicon solar cells.

Experimental Section

Materials and Contact Characterization.

Commercially available n-type Czochralski (Cz) (resistivity 1~3 Ω[?]cm) wafers were used as the substrate for all the solar cells and testing samples fabrication. SrF₂ thin films were thermally evaporated in the background vacuum under 1×10⁻³ Pa. The deposition rate is 0.1 Å[?]s⁻¹ from 99.9% purity SrF₂ powder. The film thickness is monitored by a crystal oscillator and confirmed by an ellipsometer. The composition of the SrF₂ thin films was measured by XPS and UPS. The XPS and UPS characterization was carried out on Thermo Scientific Escalab 250Xi by using the Al Kα x-ray source ($\eta\nu = 1486.6$ eV) and He I radiation ($\eta\nu = 21.22$ eV). Samples on the polished wafers were stored in the ultra-high vacuum chamber (2×10⁻⁹ mbar) over light before measurement. Surface-adventurous contamination C 1s = 284.8 eV was used to calibrate

the binding energy for the core level spectra. In order to acquire accurate secondary electron cutoffs, samples were biased -10V after a 90-second Ar⁺ ions surface clean. The cross-section images and elements distribution of the c-Si/SrF₂/Al interface were obtained using an HRTEM (JEOL JEM-2100F) combined with an EDX line scanning. A Keithley 2400 source meter and the transfer-length method (TLM) were used to test and extract the contact resistivity between various thicknesses of SrF₂ thin films on n-Si. The measurements were tested in a dark environment. The Suns- V_{oc} characterization was tested by Sinton Instruments. The asymmetric samples with SrF₂ thin films were thermally evaporated on Cz n-Si wafers (3×10^{-2} Ω[?]cm).

Cell Fabrication and Characterization.

Based on the n-type silicon substrates, the proof-of-concept 2×2 cm² solar cells were fabricated. A p-type emitter was thermally diffused by a BBr₃ source through a furnace after texturing in KOH solution and the Radio Corporation of America (RCA) standard cleaning procedure. After that, Al₂O₃/SiN_x layers for passivation and antireflection were applied to the front side of the emitter deposited by atomic layer deposition (ALD) and plasma-enhanced chemical vapor deposition (PECVD), respectively. The back surface of the solar cell was also passivated by the SiN_x layer. An array of 25 μm-diameter contact holes which account for 1% of the backside were opened with a picosecond laser. The front surface Ag metal fingers were formed by the screen-printing paste and annealing process. The solar cells were finished by a thermally evaporated Al (800 nm) or various thicknesses SrF₂/Al stack layer on the backside.

The current-voltage (J - V) measurements were carried out on Solar Cell I - V Tester (VS-6821M) under standard test conditions (25, AM 1.5G, 1000W/m²). The illumination intensity was checked by the WPVS reference solar cell. A quantum efficiency-reflection (QE-R) spectral testing instrument from Enli-tech corporation was used to characterize the external quantum efficiency (EQE) and reflectivity.

Supporting Information

Supporting Information is available from the Wiley Online Library or from the author.

Acknowledgements

This work was supported by the National Natural Science Foundation of China (Grant No. 61774173), and the Basic and Applied Basic Research Foundation of Guangdong Province (2022A1515011722).

Conflict of Interest

The authors declare no conflict of interest.

References

1. Y. Chen, H. Shen, P. P. Altermatt. Analysis of recombination losses in screen-printed aluminum-alloyed back surface fields of silicon solar cells by numerical device simulation. *Solar Energy Materials and Solar Cells*. 2014;120, 356-362. doi:<https://doi.org/10.1016/j.solmat.2013.05.051>
2. A. W. Blakers, A. Wang, A. M. Milne, J. Zhao, M. A. Green. 22.8% efficient silicon solar cell. *Applied Physics Letters*. 1989;55(13), 1363-1365. doi:10.1063/1.101596
3. P. J. Verlinden. Future challenges for photovoltaic manufacturing at the terawatt level. *Journal of Renewable and Sustainable Energy*. 2020;12(5), 1-6. doi: 10.1063/5.0020380
4. L. Cai, W. Wang, L. Jin, Z. Yao, W. Lin, et al. 12.29% low temperature-processed dopant-free cds/p-si heterojunction solar cells. *Advanced Materials Interfaces*. 2019;6(12),. doi:10.1002/admi.201900367

5. A. Richter, J. Benick, F. Feldmann, A. Fell, M. Hermle, et al. N-type si solar cells with passivating electron contact: Identifying sources for efficiency limitations by wafer thickness and resistivity variation. *Solar Energy Materials and Solar Cells*. 2017;173, 96-105. doi:10.1016/j.solmat.2017.05.042
6. T. C. Kho, K. Fong, K. McIntosh, E. Franklin, N. Grant, et al. Exceptional silicon surface passivation by an ono-dielectric stack. *Solar Energy Materials and Solar Cells*. 2019. 189,145-253. doi:10.1016/j.solmat.2018.05.061
7. J. Bullock, M. Hettick, J. Geissbuhler, A. J. Ong, T. Allen, et al. Efficient silicon solar cells with dopant-free asymmetric heterocontacts. *Nature Energy*. 2016;1. doi:10.1038/Nenergy.2015.31
8. J. Dréon, Q. Jeangros, J. Cattin, J. Haschke, L. Antognini, et al. 23.5%-efficient silicon heterojunction silicon solar cell using molybdenum oxide as hole-selective contact. *Nano Energy*. 2020;70. doi:10.1016/j.nanoen.2020.104495
9. W. Wu, W. Lin, J. Bao, Z. Liu, B. Liu, et al. Dopant-free multilayer back contact silicon solar cells employing V_2O_x /metal/ V_2O_x as an emitter. *RSC Advances*. 2017;7(38), 23851-23858. doi:10.1039/c7ra03368k
10. W. Lin, W. Wu, J. Bao, Z. Liu, K. Qiu, et al. Novel hole selective CrO_x contact for dopant-free back contact silicon solar cells. *Materials Research Bulletin*. 2018;103, 77-82. doi:10.1016/j.materresbull.2018.03.032
11. X. Yang, E. Aydin, H. Xu, J. Kang, M. Hedhili, et al. Tantalum nitride electron-selective contact for crystalline silicon solar cells. *Advanced Energy Materials*. 2018;8(20). doi:10.1002/aenm.201800608
12. S. Jackle, M. Liebhaber, C. Gerstmann, M. Mews, K. Jager, et al. Potential of PEDOT:PSS as a hole selective front contact for silicon heterojunction solar cells. *Scientific Reports*. 2017;7(1), 2170. doi:10.1038/s41598-017-01946-3
13. L. Cao, P. Procel, A. Alcañiz, J. Yan, F. Tichelaar, et al. Achieving 23.83% conversion efficiency in silicon heterojunction solar cell with ultra-thin MoO_x hole collector layer via tailoring (i)a-si:H/ MoO_x interface. *Progress in Photovoltaics: Research and Applications*. 2022. doi:10.1002/pip.3638
14. J. Bullock, P. T. Zheng, Q. Jeangros, M. Tosun, M. Hettick, et al. Lithium fluoride based electron contacts for high efficiency n-type crystalline silicon solar cells. *Advanced Energy Materials*. 2016;6(14). doi:10.1002/aenm.201600241
15. W. Wang, J. He, D. Yan, C. Samundsett, S. P. Phang, et al. 21.3%-efficient n-type silicon solar cell with a full area rear TiO_x /lif/al electron-selective contact. *Solar Energy Materials and Solar Cells*. 2020;206. doi:10.1016/j.solmat.2019.110291
16. W. Wang, J. He, L. Cai, Z. Wang, S. K. Karuturi, et al. Solution-processed electron-selective contacts enabling 21.8% efficiency crystalline silicon solar cells. *Solar RRL*. 2020;4(12). doi:10.1002/solr.202000569
17. Y. Zhang, W. Cui, Y. Zhu, F. Zu, L. Liao, et al. High efficiency hybrid PEDOT:PSS/nanostructured silicon Schottky junction solar cells by doping-free rear contact. *Energy & Environmental Science*. 2015;8(1), 297-302. doi:10.1039/c4ee02282c
18. X. Yang, Q. Bi, H. Ali, K. Davis, W. V. Schoenfeld, et al. High-performance tio_2 -based electron-selective contacts for crystalline silicon solar cells. *Advanced Materials*. 2016;28(28), 5891-5897. doi:10.1002/adma.201600926
19. Y. Wan, C. Samundsett, J. Bullock, T. Allen, M. Hettick, et al. Magnesium fluoride electron-selective contacts for crystalline silicon solar cells. *ACS Applied Material Interfaces*. 2016;8(23), 14671-14677. doi:10.1021/acsami.6b03599
20. L. Zhang, L. Meng, L. Cai, Z. Chen, W. Lin, et al. High-performance europium fluoride electron-selective contacts for efficient crystalline silicon solar cells. *Solar RRL*. 2021;5(8). doi:10.1002/solr.202100057

21. N. Chen, L. Cai, F. Xie, W. Wang, H. Wei, et al. Gadolinium fluoride as a high-thickness-tolerant electron-selective contact material for solar cells. *ACS Applied Energy Materials*. 2022;5(4), 4351-4357. doi:10.1021/acsaem.1c03919
22. W. Wang, L. Cai, L. Meng, L. Zhang, N. Chen, et al. Cerous fluoride dopant-free electron-selective contact for crystalline silicon solar cells. *Physica status solidi (RRL) -Rapid Research Letters*. 2021;15(9). doi:10.1002/pssr.202100135
23. X. Yang, P. Zheng, Q. Bi, K. Weber. Silicon heterojunction solar cells with electron selective TiO_x contact. *Solar Energy Materials and Solar Cells*. 2016;150, 32-38. doi:10.1016/j.solmat.2016.01.020
24. W. B. Ji, T. Allen, X. B. Yang, G. S. Zeng, S. De Wolf, et al. Polymeric electron-selective contact for crystalline silicon solar cells with an efficiency exceeding 19%. *ACS Energy Letters*. 2020;5(3), 897-902. doi:10.1021/acsenergylett.0c00110
25. L. Zeng, L. Cai, Z. Wang, N. Chen, Z. Liu, et al. A high-quality dopant-free electron-selective passivating contact made from ultra-low concentration water solution. *Nanomaterials (Basel)*. 2022;12(23). doi:10.3390/nano12234318
26. Z. Yao, L. Cai, L. Meng, K. Qiu, W. Lin, et al. High-performance and stable dopant-free silicon solar cells with magnesium acetylacetonate electron-selective contacts. *Physica Status Solidi-Rapid Research Letters*. 2020;14(6). doi:10.1002/pssr.202000103
27. J Bullock, Y. Wan, Z Xu, D Yan, P Phang, et al. 23% n-type crystalline silicon solar cells with TiO_x / LiF_x /Al partial rear contacts. 2018. doi:10.1109/PVSC.2018.8547414
28. Lippert, F. An introduction to toothpaste - its purpose, history and ingredients. *Monographs in Oral Science*. 2013;23. doi:10.1159/000350456
29. F. Lin, X. Liu, Y. Li, Y. Hu, X. Guo. Ultrathin metal fluoride interfacial layers for use in organic photovoltaic cells. *Advanced Functional Materials*. 2015;25(44), 6906-6912. doi:10.1002/adfm.201502871
30. S. Huang, Y. Pang, X. Li, Y. Wang, A. Yu, et al. Strontium fluoride and zinc oxide stacked structure as an interlayer in high-performance inverted polymer solar cells. *ACS Applied Material Interfaces* 2019;11(2), 2149-2158. doi:10.1021/acsaami.8b18963
31. R. P. Vasquez. SrF_2 by XPS. *Surface Science Spectra*. 1992;1(1), 24-30. doi:10.1116/1.1247687
32. J. Cho, J. Melskens, M. Debucquoy, M. Recaman Payo, S. Jambaldinni, et al. Passivating electron-selective contacts for silicon solar cells based on an a-si:H/ TiO_x stack and a low work function metal. *Progress in Photovoltaics: Research and Applications*. 2018;26(10), 835-845. doi:10.1002/pip.3023
33. V. Kanchana, G. Vaitheeswaran, M. Rajagopalan. Structural phase stability of CaF_2 and SrF_2 under pressure. *Physica B: Condensed Matter*. 2003;328(3-4), 283-290. doi:10.1016/s0921-4526(02)01851-3
34. Y. Seino, S. Yoshikawa, M. Abe, S. Morita. Growth dynamics of insulating SrF_2 films on si(111). *Journal of Physics: Condensed Matter*. 2007;19(44), 445001. doi:10.1088/0953-8984/19/44/445001
35. R. H. Cox, H. Strack. Ohmic contacts for GaAs devices. *Solid-State Electronics*. 1967;10(12), 1213. doi:10.1016/0038-1101(67)90063-9
36. Z. Chen, W. Lin, Z. Liu, L. Cai, Y. Chen, et al. Yttrium fluoride-based electron-selective contacts for crystalline silicon solar cells. *ACS Applied Energy Materials*. 2021;4(3), 2158-2164. doi:10.1021/acsaem.0c02646
37. Y. Wan, C. Samundsett, J. Bullock, M. Hettick, T. Allen, et al. Conductive and stable magnesium oxide electron-selective contacts for efficient silicon solar cells. *Advanced Energy Materials*. 2017;7(5). doi:10.1002/aenm.201601863

38. P. Shen, C. Su, Y. Lin, A. Chou, C. Cheng, et al. Ultralow contact resistance between semimetal and monolayer semiconductors. *Nature*. 2021;593(7858), 211-217. doi:10.1038/s41586-021-03472-9
39. L. G. Gerling, C. Voz, R. Alcubilla, J. Puigdollers. Origin of passivation in hole-selective transition metal oxides for crystalline silicon heterojunction solar cells. *Journal of Materials Research*. 2017;32(2), 260-268. doi:10.1557/jmr.2016.453
40. N. Chen, L. Cai, F. Xie, W. Wang, H. Wei, et al. Gadolinium fluoride as a high-thickness-tolerant electron-selective contact material for solar cells. *ACS Applied Energy Materials*. 2022;5(4), 4351-4357. doi:10.1021/acsaem.1c03919
41. Liu, Y.; Huang, Y.; Duan, X. Van der Waals integration before and beyond two-dimensional materials. *Nature* 2019;567, 323-333. doi:10.1038/s41586-019-1013-x
42. L. Zhang, L. Meng, L. Cai, Z. Chen, W. Lin, et al. High-performance europium fluoride electron-selective contacts for efficient crystalline silicon solar cells. *Solar RRL*. 2021;5(8). doi:10.1002/solr.202100057